Which-way interference within ringlike unit cells for efficient energy transfer

Davide Ferracin,[1] Andrea Mattioni,[2] Stefano Olivares,[1] Felipe Caycedo-Soler,[2,*] and Dario Tamascelli[1,2,†]
[1]*Quantum Technology Lab, Dipartimento di Fisica "Aldo Pontremoli", Università degli Studi di Milano, Via Celoria 16, 20133 Milano, Italy*
[2]*Institut für Theoretische Physik, Universität Ulm, Albert-Einstein-Allee 11, 89069 Ulm, Germany*

(Received 21 January 2019; revised manuscript received 27 March 2019; published 10 June 2019)

We show that which-way interference within ringlike unit cells enhances the propagation of electronic excitations (excitons) along linear arrays made upon these basic units. After providing an analytic approximate solution of the eigenvalue problem for such aggregates, we show that the constructive interference of wave packets leads to an excitonic population transferred across the array which is not a monotonic function of the coupling between nearest-neighbor rings. The nonmonotonicity depends on an interesting trade-off between the exciton transfer speed and the amount of energy transferred, arising from the interplay between paths within the ringlike cells and the interring coupling strength across the array.

DOI: 10.1103/PhysRevA.99.062505

I. INTRODUCTION

Solar energy conversion as a practical alternative to fossil fuels requires efficient ways to convert photons into electricity, fuel, and heat. Recently, the exact nature of the excitonic transfer within the primary steps of photosynthesis has been under close scrutiny [1–3]. Numerous experiments have revealed the presence of persistent oscillatory signals in the spectral response of different natural light harvesting antennas [4–10], including the LH2 complex of photosynthetic purple bacteria [11–13]. On the one hand, these experimental results triggered a large amount of theoretical research aimed to understand the processes that may underpin the observed long-lasting coherences [14–20]. On the other hand, they led, at first, the speculation and suggestion that light-harvesting complexes may exploit a quantum search algorithm to sample different paths simultaneously to increase speed in exciton transport [5]. This statement was contrasted with more elaborate analysis which showed that it was too far fetched for typical physiological conditions, since, for example, the transport speed between these complexes is much slower and not comparable to the scale in which dephasing, arising from the protein scaffold or solvents, restrains the endurance of oscillatory-quantum characteristics [21–23]. These speculations, however, had a positive impact as they renewed interest in the advantages for energy or information transfer provided by quantum dynamics in reduced systems [24–37] or in fully connected, disordered finite-size graphs, which, with some physical abstraction, account for motifs of nodes describing the pigments of light harvesting units [38–44].

Under the assumption of purely coherent transport, the more abstract studies on extended graphs provided valuable findings of the spatial distribution of nodes in such graphs to allow constructive interference of the transition amplitudes inducing efficient transfer from an input to an output node. These works showed [38–44] that the conjecture of a fragile efficiency from constructive interference which can be easily suppressed due to small changes in the geometry of the array (as it relies on well-defined phase relations that need to be satisfied rather accurately) could be overcome with some geometries fulfilling very basic principles. In particular, as we will specify in more detail later, it was found that graphs with an underlying centrosymmetric Hamiltonian optimize the transfer speed or amplitude. The development and the understanding of specific geometries that fulfill the principle of centrosymmetry and that are amenable to experimental implementations are of paramount importance towards the rational design of technologies making use of constructive interference.

Significant developments have been achieved in the nanofabrication of arrays that have the potential to partially display the characteristics observed in the fully quantum theoretical considerations. A large delocalization length was made possible by synthesis of self-assembled cylindrical arrays of pigments [45] or by means of implementations in synthetic systems, such as carbon-linked porphyrin nanorings [46,47]. The latter are fully π-conjugated complexes and have recently been shown to support robust quantum interference and a high degree of exciton delocalization [48–51]. Geometrically, these structures present strong similarities to the phycobilisome rodlike aggregates and the ringlike LH1 and LH2 complexes of, respectively, cyanobacteria and purple bacteria [11,52,53]. As we will consider in more detail, these systems are all circular structures or are built upon ringlike substructures which are described by centrosymmetric Hamiltonians. While the geometry and the interaction strengths in these natural or synthetic complexes may serve to explore realistic implementations, the robustness of quantum dynamics in the artificial scenarios is an interesting prospect and a motivation to explore the coherent migration of excitations across arrays of circular unit cells beyond the excitonic delocalization lengths observed in natural photosynthesis.

Following these theoretical findings and experimental achievements, we undertake the study of fully coherent

*felipe.caycedo@uni-ulm.de
†dario.tamascelli@unimi.it

excitonic propagation in arrays of structures inspired by the geometry of the basic constituents of purple bacteria photosynthetic membranes. As we show in this work, purely quantum dynamics may lead to interference of wave packets in these ringlike unit cells that is able to improve the transfer efficiency in linear arrays made upon these rings.

In the absence of aggressive noisy environments that limit the delocalization extent via dynamical processes (dephasing) or inhomogeneities (static disorder), as in natural photosynthesis, this circular configuration exhibits which-way path interference [40,54]. Namely, if a specific pigment is selectively excited, the subsequent propagation along the two available semicircular paths results in a large population in the opposite end of the ring due to the constructive interference of the propagating wave packets. In this work, we study the potential use of this interference, aiming to understand which possible ring configurations may benefit from this type of coherent excitation transfer. Our results show that linear arrays of circular structures with much less disorder than that proper of physiological environments can indeed profit from such interference phenomena for efficient energy transfer.

In more detail, we investigate and characterize the fully coherent migration of excitations along linear arrays of ringlike unit cells, whose spectral properties are explained in Sec. II. In Sec. III we provide an approximate analytical solution of the eigenvalue problem regarding linear aggregates of rings. In Sec. IV we study the dependence of the excitonic transfer speed and of the efficiency on the coupling strength between nearest-neighbor ringlike structures. We identify in particular the optimal values of such a coupling that maximize the transfer efficiency between the end points of the linear aggregate and briefly discuss the effects of dephasing and disorder. Section V is devoted to a discussion of the results, before drawing our conclusions and offering perspectives.

II. RINGLIKE UNIT CELLS

Taking inspiration from the symmetry of the purple bacteria natural antenna complexes [52], we introduce ringlike unit cells consisting of $N_D = 8$ dimeric units arranged in an N_D-cycle graph, as shown in Fig. 1; each point represents a pigment, which we model as a two-level system. In the presence of N_R such unit cells (rings), we number them with the index $r \in \{1, 2, \ldots, N_R\}$; the dimers within a ring are numbered by the index $n \in \{0, 1, \ldots, N_D - 1\}$ and the pigments in a dimer with $s \in \{1, 2\}$. We concentrate on the single-exciton manifold spanned by the states

$$|r\rangle \otimes |n\rangle \otimes |s\rangle = |r, n, s\rangle := |0\rangle \otimes \cdots \otimes \underset{(r,n,s)}{|1\rangle} \otimes \cdots \otimes |0\rangle, \tag{1}$$

representing an excited electronic state in the pigment s within the dimer n at ring r. The Hamiltonian describing the interaction between pigments within a single ring is

$$H_0 = \sum_{n=0}^{N_D-1} \sum_{s=1}^{2} E_{n,s} |n, s\rangle\langle n, s| + \sum_{n=0}^{N_D-1} J_1 (|n, 1\rangle\langle n, 2| + |n, 2\rangle\langle n, 1|) + J_2 (|n+1, 1\rangle\langle n, 2| + |n, 2\rangle\langle n+1, 1|), \tag{2}$$

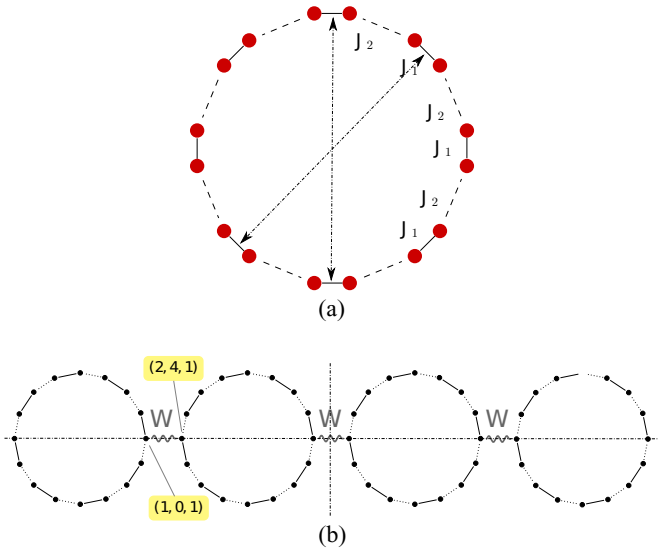

FIG. 1. (a) Geometry of the B850-mimetic ring. The intersection of the dot-dashed lines is the location of the centrosymmetry point. (b) Linear aggregate model with $N_R = 4$ and $N_D = 8$. The pigment-to-pigment coupling between nearest-neighbor rings is represented by a solid wavy line. The figure exemplifies the site numbering adopted in the paper. The centrosymmetry point of the Hamiltonian (9) is located at the intersection of the dot-dashed lines.

where we consider only the interaction between next-neighbor pigments regarding the same (J_1) or different (J_2) dimers, as shown in Fig. 1(a). The sum in (2) runs from $n = 0$ to $N_D - 1$ since, for a ring, $n = N_D$ is equivalent to $n = 0$. Using this rotational invariance of the ring Hamiltonian H_0 for identical pigments $E_{n,s} = E$, solutions for eigenenergies $\epsilon_{k,\sigma}$ and eigenvectors $|k, \sigma\rangle$ of H_0 are available [55],

$$\epsilon_{k,\sigma} = E + (-1)^\sigma \sqrt{J_1^2 + J_2^2 + 2J_1 J_2 \cos\left(\frac{2\pi k}{N_D}\right)} \tag{3}$$

$$|k, \sigma\rangle = \frac{1}{\sqrt{2}} [(-1)^\sigma e^{i\eta_k(\beta)} |k, 1\rangle + |k, 2\rangle], \tag{4}$$

where $|k, s\rangle = \sum_{n=0}^{N_D-1} \exp(i2\pi kn/N_D)|n, s\rangle/\sqrt{N_D}$ and $\eta_k(\beta) = -\arctan \frac{\sin(\frac{2\pi}{N_D}k)}{\beta+\cos(\frac{2\pi}{N_D}k)}$. Here $\beta := J_1/J_2 > 1$ indicates the degree of dimerization of the ring and sets a low ($\sigma = 1$) and a high ($\sigma = 2$) energy manifold. The energies present a pairwise degeneracy for states $|\pm k, \sigma\rangle$ except for $k = 0$ and, if N_D is even, for $k = N_D/2$. For even N_D, $k \in \{-\frac{N_D}{2}, \ldots, \frac{N_D}{2} - 1\}$, whereas for odd N_D, $k \in \{-\frac{N_D-1}{2}, \ldots, \frac{N_D-1}{2}\}$. The Hamiltonian H_0 fulfills $CH_0 = H_0C$, where C is the exchange matrix $\langle n, s|C|n', s'\rangle = \delta_{n,N_D-n'+1}\delta_{s,s'}$, and states that H_0 is centrosymmetric, i.e., invariant under mirroring with respect to the center of the matrix representation of H_0 [42–44]. This operation has a clear geometrical meaning: It corresponds to a mirror image with respect to a centrosymmetry point, as exemplified in Fig. 1(a). This property has been shown to induce constructive interference that results in dynamical revivals taking place at a site (or sites) diametrically opposed to the initialization site(s) [21,42,44,54]. Such an interference effect can be quantitatively described by the energy spectrum

of (3) which, as will be shown in the next section, remains robust even in the presence of interring interactions.

III. AGGREGATE HAMILTONIAN DIAGONALIZATION

We are interested, however, in the excitation dynamics across a linear array of N_{R} rings. It is convenient to split the Hamiltonian

$$H = \sum_{r=1}^{N_{\mathrm{R}}} |r\rangle\langle r|H_r + \sum_{r=1}^{N_{\mathrm{R}}-1} (|r\rangle\langle r+1|H_{r,r+1} + \mathrm{H.c.}) \tag{5}$$

of the full array into the interaction (2) between pigments in the same ring and the interaction

$$H_{r,r+1} = \sum_{n,s,n',s'} W_{r,n,s,r+1,n',s'} |n,s\rangle\langle n',s'| \tag{6}$$

between pigments belonging to adjacent rings.

In order to find a good approximation of the eigenstates of H, we follow a procedure similar to the one used for the solutions of the Hamiltonian in (2), however, adapted to describe a finite aggregate of rings [56], i.e., with open instead of periodic boundary conditions. This procedure can be understood as follows. We imagine the aggregate to be part of a circular, closed, chain of $M := 2N_{\mathrm{R}} + 2$ rings, in which nearest neighbors (i.e., adjacent rings) interact with an energy equal to W. We use the index r to label the elements of this extended system in such a way that the original linear aggregate occupies the positions from $r = 1$ to N_{R}; in a more graphical way, the linear aggregate of interest, connected to the auxiliary $r = 0$ and $r = N_{\mathrm{R}} + 1$ rings, forms a semicircumference of this M-ring chain. We are now in a similar situation as in the preceding section, with a Hamiltonian $\sum_{r=0}^{M-1} W(|r\rangle\langle r+1| + |r+1\rangle\langle r|)$ possessing a circular symmetry, whose eigenstates are $|\tilde{\rho}\rangle = \frac{1}{\sqrt{M}} \sum_{r=0}^{M-1} e^{i\frac{2\pi}{M}\tilde{\rho}r} |r\rangle$, $\tilde{\rho} \in \{-\frac{M}{2}, \ldots, \frac{M}{2} - 1\}$. A solution to our system requires that *any* wave function describing the actual linear array from $r = 1$ to $r = N_{\mathrm{R}}$ vanish at rings $r = 0$ and $r = N_{\mathrm{R}} + 1$ in order to satisfy the boundary conditions. This is accomplished by the set of antisymmetric combinations

$$|\rho^-\rangle := \frac{1}{\sqrt{2}}(|\tilde{\rho}\rangle - |-\tilde{\rho}\rangle), \tag{7}$$

with $\tilde{\rho} \in \{1, \ldots, N_{\mathrm{R}}\}$. These states are odd with respect to the nodes at $r = 0$ and $r = N_{\mathrm{R}} + 1$; hence the part of the wave function on the auxiliary rings from $r = N_{\mathrm{R}} + 2$ to $r = 2N_{\mathrm{R}} + 1$ is a replica of the part from $r = 1$ to $r = N_{\mathrm{R}}$, which is of the original array. Consequently, the coefficients from $r = 1$ to $r = N_{\mathrm{R}}$ suffice to describe the system, and we do not lose information if we project the $|\rho^-\rangle$ states onto the subspace spanned by $\{|r\rangle\}_{r=1}^{N_{\mathrm{R}}}$. With this procedure we obtain, normalizing the result,

$$|\rho\rangle := \sqrt{\frac{2}{N_{\mathrm{R}}+1}} \sum_{r=1}^{N_{\mathrm{R}}} \sin\left(\frac{\pi\rho r}{N_R+1}\right)|r\rangle, \tag{8}$$

with $\rho \in \{1, \ldots, N_{\mathrm{R}}\}$. These states form an orthonormal basis for the linear aggregate: They are not eigenstates of the Hamiltonian (5), but are nevertheless convenient since, as we will show, in this basis the full Hamiltonian takes a more tractable form.

In our model, presented schematically in Fig. 1(b), we assume that only the nearest pigments between adjacent rings are coupled, with an energy W, and hence

$$H_{r,r+1} = \begin{cases} W|0,1\rangle\langle\frac{N_{\mathrm{D}}}{2},1| & \text{if } N_{\mathrm{D}} \text{ is even} \\ W|0,1\rangle\langle\frac{N_{\mathrm{D}}-1}{2},2| & \text{if } N_{\mathrm{D}} \text{ is odd.} \end{cases} \tag{9}$$

This local interaction between the nearest pigments on different rings prevents diagonalization of H with the basis $\{\rho\}$. However, for identical rings ($H_r = H_0$ for all r) a change of basis from the $|r\rangle$ states to the aforementioned $|\rho\rangle$ states leads to a block-diagonal Hamiltonian $H = \bigoplus_{\rho=1}^{N_{\mathrm{R}}} h_\rho$, where

$$h_\rho = H_0 + W\cos\left(\frac{2\pi\rho}{M}\right)\hat{V}, \tag{10}$$

with $\hat{V} := (H_{r,r+1} + H_{r+1,r})/W$ [so that, by virtue of (9), $\hat{V}$ does not actually depend on r and W]. Note that the full configuration has reflection symmetry around the axes displayed in Fig. 1(b), which ensures centrosymmetry [42–44] and anticipates constructive interference taking place along the linear aggregate inducing a revival of the spreading excitonic wave function over the last ring, if the excitation is initialized in the first ring. From now on we study the adimensional Hamiltonian H_0/J_2, using J_2 as a unit of energy. We are not interested in finding the exact eigenstates of the system, but we will rather treat the interaction between the rings

$$\mathcal{V} = \xi\cos\left(\frac{2\pi\rho}{M}\right)\hat{V} = \xi_\rho\hat{V}, \tag{11}$$

having defined the dimensionless coupling constant $\xi := W/J_2$ and $\xi_\rho := \xi\cos(\frac{2\pi\rho}{M})$, as a perturbation on the single-ring Hamiltonian H_0/J_2. In the degenerate subspace $\{|\pm k,\sigma\rangle\}$ [see (4)], the interring Hamiltonian $\mathcal{V}$ takes the form $\langle k,\sigma|\mathcal{V}|\pm k,\sigma\rangle = \langle\pm k,\sigma|\mathcal{V}|k,\sigma\rangle^* = \xi_\rho\frac{(-1)^k}{N_{\mathrm{D}}}e^{-i(\eta_k(\beta)-\eta_{\pm k}(\beta))}$, with $k > 0$. Because $\eta_k(\beta) = -\eta_{-k}(\beta)$, two nondegenerate eigenvectors arise for each positive value of k, which we label with the index $\nu \in \{1,2\}$. The eigenvalues of this matrix, namely, the first-order corrections to the single-ring energies from (3), are $\xi_\rho\Delta\epsilon^{(1)}_{k,\sigma,\nu}$, where

$$\Delta\epsilon^{(1)}_{k,\sigma,\nu} = \begin{cases} (-1)^k\frac{2}{N_{\mathrm{D}}}\delta_{\nu,2} & \text{if } N_{\mathrm{D}} \text{ is even} \\ \frac{(-1)^{\sigma+k}}{N_{\mathrm{D}}}\left\{\cos\left[\frac{\pi k}{N_{\mathrm{D}}} + \eta_k(\beta)\right] + (-1)^\nu\right\} & \text{if } N_{\mathrm{D}} \text{ is odd.} \end{cases} \tag{12}$$

The perturbed eigenvalues are clearly dependent on the interring coupling strength W. The eigenvectors of $\mathcal{V}$ in the degenerate subspace $\{|\pm k,\sigma\rangle\}$ are labeled $|k,\sigma,\nu\rangle$ and are independent of W; they can be used to obtain the new eigenstates $|\rho\rangle|k,\sigma,\nu\rangle$ of the aggregate with N_R rings. Following this procedure, we obtain, for N_{D} even,

$$|\rho,k,\sigma,\nu\rangle = \frac{1}{\sqrt{2}}|\rho\rangle[(-1)^\nu e^{-2i\eta_k(\beta)}|k,\sigma\rangle + |-k,\sigma\rangle], \tag{13}$$

while for N_{D} odd,

$$|\rho,k,\sigma,\nu\rangle = \frac{1}{\sqrt{2}}|\rho\rangle[(-1)^\nu e^{i(\pi k/N_{\mathrm{D}})-i\eta_k(\beta)}|k,\sigma\rangle + |-k,\sigma\rangle]. \tag{14}$$

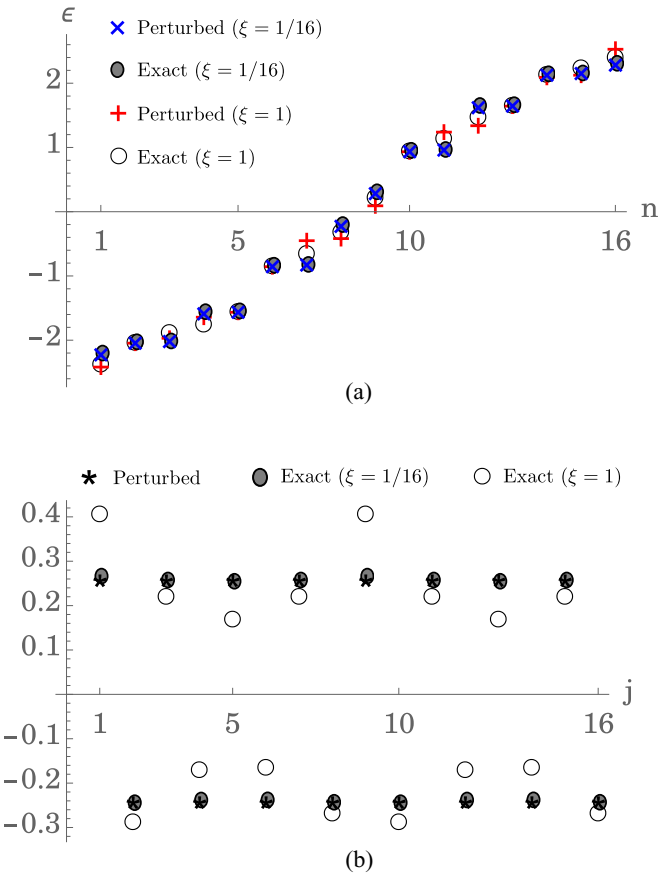

FIG. 2. Comparison between the exact (numerical) and approximate perturbative diagonalization for an aggregate of $N_R = 4$ rings of $N_D = 8$ dimers for different values of the interring coupling strength $\xi = W/J_2$; each ring is parametrized as in Fig. 1. (a) Eigenvalues of the $\rho = 1$ block of the Hamiltonian (10). (b) Amplitudes $\phi_{n,s}$ of the eigenstate $|\phi\rangle = \sum_{n,s} \phi_{n,s}|n, s\rangle$ of the same $\rho = 1$ block of the Hamiltonian (10) corresponding to the lowest energy (ground state of the $\rho = 1$ block) for the index mapping $j = N_D(n-1) + s$.

To establish an analysis with the prospect of future implementations, we use the couplings obtained from optical measurements in the B850 ring of the LH2 complex of purple bacteria [57]: $J_1 = 320\ \mathrm{cm}^{-1}$ and $J_2 = 255\ \mathrm{cm}^{-1}$. As shown in Fig. 2(a), referring to the manifold $\rho = 1$, for small ξ the structure of degenerate doublets ordered in a high- and a low-energy submanifold given by (3) remains, and the result of numerical diagonalization is pretty close to that of the perturbed analysis. Interestingly, the perturbative analysis is off the numerical diagonalization by at most 10% (relative error) for interring interactions as large as intraring interactions, as shown for $\xi = 1$ in Fig. 2(a). Hence, as long as the eigenvalues are concerned, the approximation obtained by the perturbative analysis is very good. The perturbed eigenstates, on the other hand, are in worse agreement with the numerically exact eigenstates, as shown for the amplitudes of the lowest-energy state in Fig. 2(b). However, since the perturbation is proportional to $\cos(\frac{2\pi\rho}{M})$, it acquires its maximum value for the manifold of lowest energy $\rho = 1$, so this selected case represents the worst-case scenario among all manifolds. The other manifolds will present even smaller corrections; we can thus safely address the indices (k, σ) as good quantum numbers for single-ring states, even when we consider *all* the interactions of the Hamiltonian H.

IV. CHARACTERIZATION OF THE EXCITATION TRANSFER PROCESS

We label the eigenstates of H as $|e_\mu\rangle$, in ascending order of energy ϵ_μ for larger indices $\mu \in \{1, \ldots, 2N_D N_R\}$. With these eigenstates and eigenvalues, we can approach the study of the time evolution $|\psi(t)\rangle = \exp(-iHt)|\psi_0\rangle$ of an initial state $|\psi_0\rangle$. In particular, the probability that the excitation is found in the rth ring at time t is given by

$$P_r(t) = \sum_{n,s} |\langle r, n, s| \exp(-iHt)|\psi_0\rangle|^2 = \sum_{\mu,\mu'} e^{i(\epsilon_{\mu'} - \epsilon_\mu)t} \langle e_{\mu'}|\pi_r|e_\mu\rangle\langle e_\mu|\psi_0\rangle\langle\psi_0|e_{\mu'}\rangle, \quad (15)$$

where $\pi_r = |r\rangle\langle r| \otimes \sum_{n,s} |n, s\rangle\langle n, s|$. Due to the identification of the states $|k, \sigma\rangle$ from (4) as being appropriate for the description of the rings in the chain, this projector can also be written as $\pi_r = |r\rangle\langle r| \otimes \sum_{k,\sigma} |k, \sigma\rangle\langle k, \sigma|$. This approximation is based on the robustness of single-ring states to the interring interaction discussed in Fig. 2 and permits postulating $|e_\mu\rangle \approx |\rho, k, \sigma, \nu\rangle$ as an approximation for the full array eigenstates. Accordingly, the relation $\langle e_{\mu'}|\pi_r|e_\mu\rangle \approx \delta_{k',k}\delta_{\sigma',\sigma}\delta_{\nu',\nu}\langle\rho'|r\rangle\langle r|\rho\rangle$ follows. This results in

$$P_r(t) \approx \sum_{\rho,\rho',k,\sigma,\nu} e^{i(\epsilon_{\rho',k,\sigma,\nu} - \epsilon_{\rho,k,\sigma,\nu})t} \langle\rho'|r\rangle\langle r|\rho\rangle \times \langle\rho, k, \sigma, \nu|\psi_0\rangle\langle\psi_0|\rho', k, \sigma, \nu\rangle, \quad (16)$$

which together with the solutions (12) and (13) represents the perturbative solution for the dynamics of ring populations. In the following we will consider situations in which only the leftmost ring ($r = 1$) is initially populated and we write the initial state as $|\psi_0\rangle = |r = 1\rangle|\phi\rangle$, where $|\phi\rangle$ is a yet unspecified single-ring state.

In Fig. 3 we present the time evolution of the populations in a linear aggregate of four rings, for different values of ξ and using the same parameters we chose for the eigenvalues and eigenstates of Fig. 2. First, notice that the solution from numerical diagonalization for ξ equal to $\frac{1}{16}$ or $\frac{1}{4}$ presented in Figs. 3(a) and 3(b), respectively, is very similar to the perturbative solution which is shown in Fig. 3(d) for $\xi = \frac{1}{16}$. Second, note that all the results in this figure present similar characteristics for different values of ξ when they are displayed as a function of the timescale $t\xi$. This can be understood from P_r in (16), which depends on time solely through the argument $t(\epsilon_{\rho,k,\sigma,\nu} - \epsilon_{\rho',k,\sigma,\nu})$. A good approximation of $\epsilon_{\rho,k,\sigma,\nu} - \epsilon_{\rho',k,\sigma,\nu} \approx (\xi_\rho - \xi_{\rho'})\Delta\epsilon^{(1)}_{k,\sigma,\nu}$ is found from (12) which, based on the definition of ξ_ρ in (11), states $\epsilon_{\rho,k,\sigma,\nu} - \epsilon_{\rho',k,\sigma,\nu} \propto W$, i.e., the timescale of transfer across the array is mainly given by the interring coupling W and does not depend at first order on the details of the ring dynamics, due to the robustness of the single-ring excitonic manifold.

The speed of transfer is a complementary measure to the transfer efficiency to characterize the performance for energy transfer [38,39]. A measure for the transfer efficiency

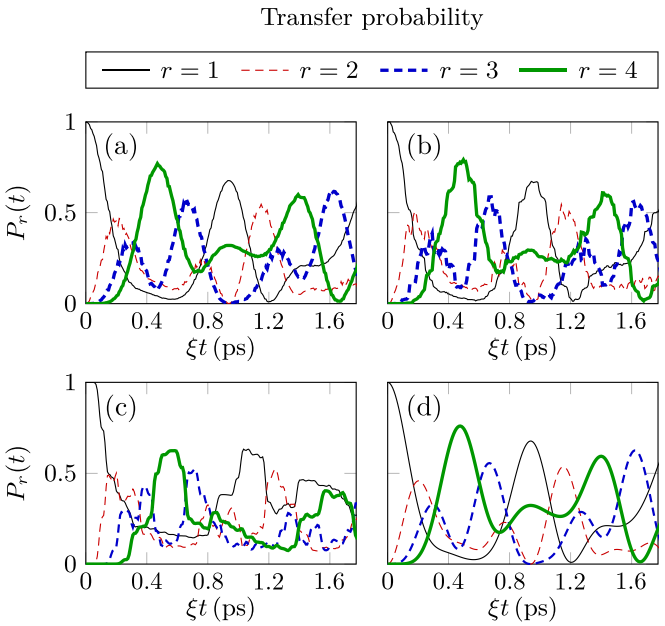

FIG. 3. Time evolution of populations in an aggregate of $N_R = 4$ rings, when initially the excitation is in the leftmost site of the first ring ($|\phi\rangle = |n = 4, s = 1\rangle$) for different values of the interring coupling $\xi = W/J_2$: (a) $\xi = \frac{1}{16}$, (b) $\xi = \frac{1}{4}$, and (c) $\xi = 1$. (d) Result of the perturbative analysis for $\xi = \frac{1}{16}$. In all the panels a rescaled time ξt (ps) is used.

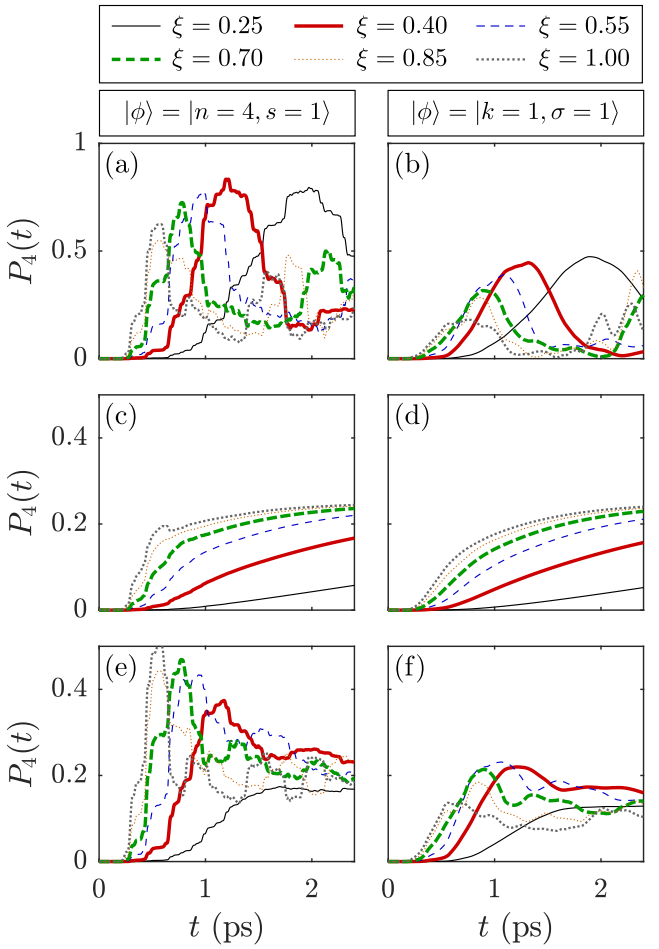

FIG. 4. Transfer efficiency as a function of time for different values of the rescaled interring coupling $\xi = W/J_2$ in an array of four rings: (a) exciton in the leftmost site of the first ring of the array, i.e., $|\phi\rangle = |n = 4, s = 1\rangle$; (b) delocalized initial condition $|\phi\rangle = |k = 1, \sigma = 1\rangle$; (c) and (d) effect of dephasing ($\Gamma = 0.1J_2$) on the dynamics of the transfer efficiency $P_4(t)$ for the same initial state as in (a) and (b), respectively; and (e) and (f) effect of static disorder ($\Delta = 0.1J_2$, with 10^3 stochastic realizations) on the dynamics of the transfer efficiency $P_4(t)$ for the same initial state as in (a) and (b), respectively. In all cases, the system is initialized in the first ring: $|\psi_0\rangle = |r = 1\rangle|\phi\rangle$.

considered in a previous analysis [38,39] is the maximal output probability, which in our case regards the maximum occupation probability P_{N_R} at the last ring. This measure quantifies transfer within the molecular network from the input to the output site. The transfer is regarded as successful if the excitation reaches the output site with high probability in a short time [38,39].

Following the solution to the first-order perturbation on ξ, addressing the degenerate manifold $\{|\pm k, \sigma\rangle\}$, we find that the efficiency $P_{N_R}(t) \approx P^{(1)}_{N_R}(t) = f(2\xi t/N_D)$, where f is a non-negative smooth function (see the Appendix for details). It follows that, as long as ξ remains small, the timescale of transfer is given approximately by $1/\xi$ as obtained in Fig. 3. In this regime, therefore, the details of the ring Hamiltonian, e.g., the dimerization degree $\beta = J_1/J_2$, are not important to determine the properties of the transfer along the aggregate.

Notice in Fig. 3(c), and in more detail in Fig. 4(a), that the height of the first revival in the fourth ring becomes smaller as the value of ξ increases. In order to explain this, we need to consider second-order corrections in ξ. As it will be shown next, while at first order the perturbation only lifts the degeneracies within the manifolds $\{|\pm k, \sigma\rangle\}$, higher-order contributions mix states from nondegenerate manifolds, introducing in (15) an additional dependence on ξ of the amplitudes of the transferred populations.

We can explicitly see this additional ξ dependence by considering the effect of the interring coupling on two non-degenerate subspaces $\{|\pm k_1, \sigma\rangle\}$ and $\{|\pm k_2, \sigma\rangle\}$ such that $\langle k_1, \sigma|\hat{V}|k_2, \sigma\rangle \neq 0$ and solving the dynamics in this four-dimensional subspace only. For this reduced subspace, we obtain the expression

$$P_{N_R}(t) \approx \frac{2}{N_D}\left(f(2\xi t/N_D) + \frac{2\xi^2}{N_D^2\delta^2} f''(2\xi t/N_D)\right), \qquad (17)$$

valid to lowest nonzero order in ξ, where $\delta = (\epsilon_{k_1,\sigma} - \epsilon_{k_2,\sigma})/J_2$ (see the Appendix for details). To first order in ξ, P_{N_R} reaches a maximum when the first derivative of f is zero and the second derivative f'' is negative. Therefore, from (17) we see that the interring coupling has two effects: On the one hand it compresses the transfer timescale through the argument $2\xi t/N_D$ of f, while on the other it reduces the amplitude of P_{N_R} by an amount proportional to f''. Notice that the difference in energy δ depends on the details of the ring, as provided by (3), so it follows that the amplitude of the transfer can be devised upon the details of the ring interactions. It turns out then that the speed (depending on the

coupling strength between rings) and amplitude (depending on the geometrical details and couplings within each ring) of the transferred population maximize to an optimum point, as expected from concurrent quantities.

To better resolve this optimal value, Fig. 4(a) shows that the amplitude of the transferred population starts to decrease appreciably when $0.4 \lesssim \xi \lesssim 0.5$, while the time required to reach the maximum population in the fourth ring decreases from about 1.2 to 1 ps. A further increase to $\xi = 0.7$ reduces this time to 0.8 ps at the expense of reducing about 15% the amplitude of the last ring population. Changes of the ring geometry or interactions may suppress this reduction, but a specific set of parameters can be better implemented if additional dissipation processes that may avoid the successful transfer to the end of the chain are incorporated.

In order to shed light on the phenomenon involving the variable amount of population transferred to the last ring, in Fig. 4 we compare the population transferred to the last ring when the first ring is initialized on a single pigment [Fig. 4(a)] or delocalized over the full ring [Fig. 4(b)]. A rigorous treatment of initialization would require us to explicitly consider the interaction with optical fields, which extends beyond the single-excitation manifold spanned by the states defined in (1) and would divert the scope of our analysis. However, the optical response to continuous illumination of the ringlike geometry considered is well described by the transition dipole strength of the states $|k, \sigma\rangle$ [58], which are significant only for the states $|k = \pm 1, \sigma = 1\rangle$, which we will refer to as bright states. This fact supports our choice of $|\phi\rangle$ for Fig. 4(b). A practical implementation of the initial condition studied in Fig. 4(a) would require optical pulses much shorter than the timescale of intraring coherent propagation (much shorter than $2\pi/J_1$) and directed towards the location of individual pigments. Nowadays, the routine use of pulses with duration of a few femtoseconds [4–13] easily lifts the restriction imposed by the magnitude of J_1, whereas evanescent fields may nowadays offer a prospect of a spatial resolution of approximately 5–10 nm for selective excitation [59,60], which is nevertheless still larger than the approximately 1-nm separation between adjacent pigment in the circular structures mentioned in the Introduction. Thereby, spatial resolution is a major obstacle for a realistic implementation of initialization in a single pigment. As it can be observed, the single-pigment initialization leads to a much higher transfer efficiency than the delocalized $|k = 1, \sigma = 1\rangle$ initialization.

We now introduce $P_{N_R}^{n,s}$ and $P_{N_R}^{k,\sigma}$ to analyze the transfer efficiency in the last ring arising from initializations in a site $|\phi\rangle = |n, s\rangle$ or in a delocalized exciton $|\phi\rangle = |k, \sigma\rangle$, respectively, as indicated by the superscripts. Using these initial states in (15), it is straightforward to show (see the Appendix) that initialization in the leftmost or rightmost pigments on the first ring in Fig. 1, $|\phi\rangle = |n = 0, s = 1\rangle$ or $|\phi\rangle = |n = \frac{N_D}{2}, s = 1\rangle$, results in a population at the last ring which doubles the one arising from the initialization at the bright delocalized state $|\phi\rangle = |k = 1, \sigma = 1\rangle$, i.e., $P_{N_R}^{n=4,s=1}(t) = P_{N_R}^{n=0,s=1}(t) = 2P_{N_R}^{k=1,\sigma=1}(t)$. It can also be shown that the transfer efficiency is the same for any other $|\phi\rangle = |k, \sigma\rangle$ state, which allows writing $P_{N_R}^{n=4,s=1}(t) = P_{N_R}^{n=0,s=1}(t) = 2P_{N_R}^{k,\sigma}(t)$. Moreover, it also follows from (15) that initialization in any pigments other than those lying along the linear aggregate axis leads to a transfer efficiency which is the same as that from the delocalized states $|\phi\rangle = |k, \sigma\rangle$. Thereby, the equalities $P_{N_R}^{n=4,s=1}(t) = P_{N_R}^{n=0,s=1}(t) = 2P_{N_R}^{k,\sigma}(t)$ underlie that initialization in the first ring from any pigments other than those lying along the linear aggregate axis or on fully delocalized states leads to a reduced transfer probability with respect to that after initialization in pigments lying along the linear aggregate axis. Then a physical picture emerges where the optimal transfer efficiency occurs when initialization in $|\phi\rangle = |n = 4, s = 1\rangle$ or $|\phi\rangle = |n = 0, s = 1\rangle$, followed by propagation in two wavefronts along the branches of the ring, results in constructive interference at the site coupled to the neighboring ring.

Notice, however, that the effect will be attributed to both the which-way propagation within each ringlike unit cell and the particular form of the interring coupling specified in (9). The latter allows, as the dynamics proceeds, excitations to reach initially a single pigment on intermediate rings. This local initialization of intermediate rings will result in constructive which-way interference within intermediate rings, which might enhance transfer. Thereby, the reduction $P_{N_R}^{k,\sigma}(t) = \frac{1}{2}P_{N_R}^{n=4,s=1}(t) = \frac{1}{2}P_{N_R}^{n=0,s=1}(t)$ can be attributed to the internal dynamics of the first ring, while an additional reduction should arise if the interference in the intermediate rings is somehow hindered.

To illustrate this point, we calculate the dynamics of the linear aggregate in the presence of dephasing between pigments. In short, we evolve the density operator ϱ according to $\partial_t \varrho = -i[H, \varrho] + \Gamma \sum_{r,n,s}(|r, n, s\rangle\langle r, n, s|\varrho|r, n, s\rangle\langle r, n, s| - \varrho)$, where $\Gamma/2$ describes the dephasing rate between the ground and the excited state of pigment r, n, s. The results in Fig. 4(c) show that for $\xi = 1$ and $2\pi W > \Gamma$ the oscillatory dynamics results in a maximum population at the last ring (approximately equal to 0.2) which is considerably smaller than the analogous quantity in the fully coherent case [approximately equal to 0.6; see Fig. 4(a)]. Thereby, decoherence within pigments decreases the peak population in the last ring, which underlines the importance of constructive interference within each ring to accomplish efficient transfer. No qualitative differences are observed when choosing a delocalized initial condition over the leftmost ring, as can be seen from Fig. 4(d).

We also test the robustness of the transfer mechanism described above against static disorder. We randomly perturb the pigment energies E by an amount $\delta E_{r,n,s}$ sampled from a zero-mean Gaussian distribution with standard deviation Δ and look at the ensemble-averaged dynamics. The results in Figs. 4(e) and 4(f) show that for both single-site (the leftmost pigment of the first ring) and delocalized (on the first ring) initialization, static disorder reduces the maximum population transferred to the last ring. A comparison with the noiseless scenario shown in Figs. 4(a) and 4(b) highlights that the reduction is more severe for smaller interring couplings ($\xi = 0.25$), as it might be expected from Anderson localization [61], which predicts larger backscattering of the wavefront for larger values of Δ/ξ. In the case of a single-site initial state, the scattering of the wave function results in both larger and faster population transfer to the last ring. In contrast, the case of a delocalized initial state in the first ring shows a

smaller population on the last ring and a faster propagation as the coupling is increased ($\xi \gtrsim 0.4$) for the same level of disorder. Since the trade-off of faster but smaller population transferred for increasing interring coupling was observed in the noiseless scenarios (site and delocalized initialization), this hints towards a more robust transfer against the scattering of the wave packet when the system is initially in a delocalized state. We ascribe this stability against disorder to the proven robustness of delocalized excitons against static noise, which leads to the well-known exchange narrowing mechanism [58], i.e., local fluctuations on sites $|n, s\rangle$ map onto smaller fluctuations on excitons $|k, \sigma\rangle$. Heuristically, this robustness can be understood in terms of the absence of which-way interference in the first ring for the delocalized initialization with or without static disorder, which is present in the noiseless case for single-site initial excitation but is disrupted by disorder.

V. CONCLUSION

Motivated by the apparent symmetry of natural harvesting structures and by the characteristics of available synthetic platforms, we investigated the effect of short-range interactions and dynamics within ringlike unit cells on the long-range propagation of excitations in linear aggregates of these basic units. In a scenario where intraring interactions are stronger than interring couplings, we studied the situation in which only the closest pigments of nearest-neighbor rings in the aggregate interact with each other. We obtained an analytic approximate solution of the eigenvalue problem for the system Hamiltonian by means of a perturbative approach on the interring coupling strength, which enabled us to illustrate that interring coupling is the only quantity that sets the timescale for coherent population exchange between rings, while the geometry of the unit cells may result in a beneficial constructive interference of wave packets in the spatial locations where the interaction among unit cells is strongest.

Even though the specific conditions to observe the advantages of constructive interference in unit cells might be challenging at present, this work aims to foster the investigation of quantum mechanical dynamics within unit cells for optimization of transfer at larger scales, as expressed with the multichromophoric Förster theory formalized years ago by Jang *et al.* [62] and more recently to understand the diffusion lengths observed in nanoengineered arrays of purple bacteria complexes [63,64].

ACKNOWLEDGMENTS

We thank Susana F. Huelga and Martin B. Plenio for many useful discussions. This work was supported by the ERC Synergy grant BioQ and the IQST, as well as a grant from the John Templeton Foundation.

APPENDIX: PERTURBATIVE EXPRESSION OF THE TRANSFER PROBABILITY

The starting point for the calculation of the transfer probability $P_{N_R}(t)$ is (15). Writing the aggregate's eigenstates as $|e_\mu\rangle = |\rho\rangle|\kappa_\rho\rangle$ allows us to rewrite (15) for the last ring $r = N_R$ as

$$P_{N_R}(t) = \sum_{\rho,\rho'} (-1)^{\rho+\rho'} |\langle r = 1|\rho\rangle|^2 |\langle r = 1|\rho'\rangle|^2 \times \sum_{\kappa,\kappa'} e^{i(\epsilon_{\rho\kappa} - \epsilon_{\rho'\kappa'})t} \langle\phi|\kappa_\rho\rangle\langle\kappa_\rho|\kappa'_{\rho'}\rangle\langle\kappa'_{\rho'}|\phi\rangle. \quad \text{(A1)}$$

This is justified by the block-diagonal structure of the aggregate's Hamiltonian, which results in eigenstates $\{|\epsilon_\mu\rangle\}_\mu = \{|\rho\rangle|\kappa_\rho\rangle\}_{\rho,\kappa}$. The states $|\kappa_\rho\rangle$ are eigenstates of the ρth block h_ρ, as defined in (10), with eigenvalues $\epsilon_{\rho,\kappa}$. The subscript ρ indicates that the amplitudes may depend parametrically on the perturbation ξ_ρ. At first order in ξ, $\{|\kappa_\rho\rangle\}_{\kappa,\rho} = \{|k, \sigma, \nu\rangle\}_{k,\sigma,\nu}$ and the overlap $\langle\kappa_\rho|\kappa'_{\rho'}\rangle = \delta_{k,k'}\delta_{\sigma,\sigma'}\delta_{\nu,\nu'}$ does not depend on ρ. However, for higher orders $\langle\kappa_\rho|\kappa'_{\rho'}\rangle$ will be largest for $\rho = \rho'$. This orthogonality condition between the states $|\kappa_\rho\rangle$, realized at first order in ξ, renders the calculation of the first term in (17) straightforward and yields the result $P_{N_R}(t) \approx f(2\xi t/N_D)$, with

$$f(x) = \left| \sum_\rho (-1)^\rho |\langle 1|\rho\rangle|^2 e^{ix\cos[\pi\rho/(N_R+1)]} \right|^2. \quad \text{(A2)}$$

The calculation can be repeated considering an initially localized state on the first ring

$$P^{n,s}_{N_R}(t) = \left| \sum_\rho (-1)^\rho |\langle 1|\rho\rangle|^2 e^{i(2/N_D)\xi_\rho t} \right|^2 \quad \text{(A3)}$$

or delocalized in a single-ring eigenstate $|k, \sigma\rangle$, which results in the relation

$$P^{k,\sigma}_{N_R}(t) = \tfrac{1}{2} P^{n,s}_{N_R}(t). \quad \text{(A4)}$$

The calculations are more involved when we consider second-order mixing between nondegenerate manifolds. In this case we compute the dynamics only within a four-dimensional subspace given by two degenerate manifolds $\{|\pm k_1, \sigma\rangle\}$ and $\{|\pm k_2, \sigma\rangle\}$. Projecting (10) on this subspace, one sees that only two of the four first-order eigenstates couple, namely, $\{|i\rangle = \langle\rho|\rho, k_i, \sigma, 2\rangle\}_{i=1,2}$ [cf. Eqs. (10) and (11)]. These result in the κ_ρ states

$$|+_\rho\rangle = e^{i(\eta_{k_1} - \eta_{k_2})} \cos\theta_\rho |1\rangle + \sin\theta_\rho |2\rangle, \quad \text{(A5)}$$

$$|-_\rho\rangle = -e^{i(\eta_{k_1} - \eta_{k_2})} \sin\theta_\rho |1\rangle + \cos\theta_\rho |2\rangle, \quad \text{(A6)}$$

with eigenvalues $\epsilon_{\rho,\pm} = 2\xi_\rho/N_D \pm \frac{1}{2}\sqrt{\delta^2 + (4\xi_\rho/N_D)^2}$, where the mixing angle is given by $\theta_\rho = \frac{1}{2}\arctan\frac{4\xi_\rho}{N_D\delta}$. Plugging (A5) and (A6) into (A1) gives rise to some terms oscillating at a frequency $O(\delta)$, which is larger than the end-to-end transfer frequency $O(\xi)$. Therefore, we perform a rotating-wave approximation by retaining only the terms that oscillate with a frequency of order ξ. At this point, expanding the mixing angles to second order in ξ, one obtains the final expression (17), showing the explicit dependence of the probability on the last ring on the perturbative parameter.

[1] G. Scholes, G. Fleming, L. Chen, A. Aspuru-Guzik, A. Buchleitner, D. Coker, G. Engel, R. Van Grondelle, A. Ishizaki, D. Jonas, J. Lundeen, J. McCusker, S. Mukamel, J. Ogilvie, A. Olaya-Castro, M. Ratner, F. Spano, K. Whaley, and X. Zhu, Nature (London) **543**, 647 (2017).

[2] E. Romero, V. I. Novoderezhkin, and R. van Grondelle, Nature (London) **543**, 355 (2017).

[3] S. F. Huelga and M. B. Plenio, Contemp. Phys. **54**, 181 (2013).

[4] T. Brixner, J. Stenger, H. M. Vaswani, M. Cho, R. E. Blankenship, and R. G. Fleming, Nature (London) **434**, 625 (2005).

[5] G. S. Engel, T. R. Calhoun, E. L. Read, T. K. Ahn, T. Mancal, Y. C. Cheng, R. E. Blankenship, and G. R. Fleming, Nature (London) **446**, 782 (2007).

[6] H. Lee, Y.-C. Cheng, and G. R. Fleming, Science **316**, 1462 (2007).

[7] E. Collini, C. Y. Wong, K. E. Wilk, P. M. G. Curmi, P. Brumer, and G. D. Scholes, Nature (London) **463**, 644 (2010).

[8] G. Panitchayangkoon, D. Hayes, K. A. Fransted, J. R. Caram, E. Harel, J. Wen, R. E. Blankenship, and G. S. Engel, Proc. Natl. Acad. Sci. USA **107**, 12766 (2010).

[9] B. S. Rolczynski, H. Zheng, V. P. Singh, P. Navotnaya, A. R. Ginzburg, J. R. Caram, K. Ashraf, A. T. Gardiner, S.-H. Yeh, S. Kais, R. J. Cogdell, and G. S. Engel, Chem **4**, 138 (2018).

[10] M. Maiuri, E. Ostroumov, R. G. Saer, R. Blankenship, and G. D. Scholes, Nat. Chem. **10**, 177 (2018).

[11] E. Harel and G. S. Engel, Proc. Natl. Acad. Sci. USA **109**, 706 (2012).

[12] R. Hildner, D. Brinks, J. B. Nieder, R. J. Cogdell, and N. F. van Hulst, Science **340**, 1448 (2013).

[13] A. F. Fidler, V. P. Singh, P. D. Long, P. D. Dahlberg, and G. S. Engel, Nat. Commun. **5**, 3286 (2014).

[14] A. Ishizaki and G. R. Fleming, Proc. Natl. Acad. Sci. USA **106**, 17255 (2009).

[15] A. W. Chin, J. Prior, R. Rosenbach, F. Caycedo-Soler, S. F. Huelga, and M. B. Plenio, Nat. Phys. **9**, 113 (2013).

[16] N. Christensson, H. F. Kauffmann, T. Pullerits, and T. Mančal, J. Phys. Chem. B **116**, 7449 (2012).

[17] V. Tiwari, W. K. Peters, and D. M. Jonas, Proc. Natl Acad. Sci. USA **110**, 1203 (2013).

[18] J. M. Womick and A. M. Moran, J. Chem. Phys. B **115**, 1347 (2011).

[19] F. Caycedo-Soler, A. W. Chin, J. Almeida, S. F. Huelga, and M. B. Plenio, J. Chem. Phys. **136**, 155102 (2012).

[20] A. Kolli, E. J. O'Reilly, G. D. Scholes, and A. Olaya-Castro, J. Chem. Phys. **137**, 174109 (2012).

[21] F. Levi, S. Mostarda, F. Rao, and F. Mintert, Rep. Prog. Phys. **78**, 082001 (2015).

[22] J. Strümpfer and K. Schulten, J. Chem. Phys. **137**, 065101 (2012).

[23] S. M. Blau, D. I. G. Bennett, C. Kreisbeck, G. D. Scholes, and A. Aspuru-Guzik, Proc. Natl. Acad. Sci. U.S.A. **115**, E3342 (2018).

[24] R. J. Sension, Nature (London) **446**, 740 (2007).

[25] A. Olaya-Castro, C. F. Lee, F. F. Olsen, and N. F. Johnson, Phys. Rev. B **78**, 085115 (2008).

[26] M. Plenio and S. Huelga, New J. Phys. **10**, 113019 (2008).

[27] M. Sarovan, A. Ishizaki, G. Fleming, and K. Whaley, Nat. Phys. **6**, 462 (2010).

[28] C. Smyth, F. Fassioli, and G. Scholes, Philos. Trans. R. Soc. A **370**, 3728 (2012).

[29] S. Sangwoo, P. Rebentrost, S. Valleau, and A. Aspuru-Guzik, Biophys. J. **102**, 649 (2012).

[30] M. Mohseni, P. Rebentrost, S. Lloyd, and A. Aspuru-Guzik, J. Chem. Phys. **129**, 174106 (2008).

[31] E. K. Irish, R. Gómez-Bombarelli, and B. W. Lovett, Phys. Rev. A **90**, 012510 (2014).

[32] M. del Rey, A. W. Chin, S. F. Huelga, and M. B. Plenio, J. Phys. Chem. Lett. **4**, 903 (2013).

[33] A. Childs, E. Farhi, and S. Gutmann, Quantum Inf. Process. **1**, 35 (2002).

[34] A. M. Childs, R. Cleve, E. Deotto, E. Farhi, S. Gutmann, and D. A. Spielman, *Proceedings of the 35th Annual ACM Symposium on Theory of Computing, San Diego, 2003* (ACM, New York, 2003), pp. 59–68.

[35] M. Christandl, N. Datta, T. C. Dorlas, A. Ekert, A. Kay, and A. J. Landahl, Phys. Rev. A **71**, 032312 (2005).

[36] D. Tamascelli, S. Olivares, S. Rossotti, R. Osellame, and M. G. A. Paris, Sci. Rep. **6**, 26054 (2016).

[37] S. Bose, Contemp. Phys. **48**, 13 (2007).

[38] T. Scholak, F. de Melo, T. Wellens, F. Mintert, and A. Buchleitner, Phys. Rev. E **83**, 021912 (2011).

[39] T. Scholak, T. Wellens, and A. Buchleitner, J. Phys. B **44**, 184012 (2011).

[40] O. Mülken and A. Blumen, Phys. Rep. **502**, 37 (2011).

[41] S. Mostarda, F. Levi, D. Prada-Gracia, F. Mintert, and F. Rao, Nat. Commun. **4**, 2296 (2013).

[42] M. Walschaers, J. F.-d.-C. Diaz, R. Mulet, and A. Buchleitner, Phys. Rev. Lett. **111**, 180601 (2013).

[43] T. Zech, R. Mulet, T. Wellens, and A. Buchleitner, New J. Phys. **16**, 055002 (2014).

[44] M. Walschaers, R. Mulet, T. Wellens, and A. Buchleitner, Phys. Rev. E **91**, 042137 (2015).

[45] J. Lim, D. Paleček, F. Caycedo-Soler, C. N. Lincoln, J. Prior, H. von Berlepsch, S. F. Huelga, M. B. Plenio, D. Zigmantas, and J. Hauer, Nat. Commun. **6**, 7755 (2015).

[46] M. C. O'Sullivan, J. K. Sprafke, D. V. Kondratuk, C. Rinfray, T. D. W. Claridge, A. Saywell, M. O. Blunt, J. N. O'Shea, P. H. Beton, M. Malfois, and H. L. Anderson, Nature (London) **469**, 72 (2011).

[47] D. V. Kondratuk, J. K. Sprafke, M. C. O'Sullivan, L. M. A. Perdigao, A. Saywell, M. Malfois, J. N. O'Shea, P. H. Beton, A. L. Thompson, and H. L. Anderson, Chem. Eur. J. **20**, 12826 (2014).

[48] S. Richert, J. Cremers, I. Kuprov, M. D. Peeks, H. L. Anderson, and C. R. Timmel, Nat. Commun. **8**, 14842 (2017).

[49] M. Rickhaus, A. Vargas Jentzsch, L. Tejerina, I. Grübner, M. Jirasek, T. D. W. Claridge, and H. L. Anderson, J. Am. Chem. Soc. **139**, 16502 (2017).

[50] C.-K. Yong, P. Parkinson, D. V. Kondratuk, W.-H. Chen, A. Stannard, A. Summerfield, J. K. Sprafke, M. C. O'Sullivan, P. H. Beton, H. L. Anderson, and L. M. Herz, Chem. Sci. **6**, 181 (2015).

[51] P. Parkinson, D. V. Kondratuk, C. Menelaou, J. Q. Gong, H. L. Anderson, and L. M. Herz, J. Phys. Chem. Lett. **5**, 4356 (2014).

[52] S. Scheuring, J. L. Rigaud, and J. N. Sturgis, EMBO J. **23**, 4127 (2004).

[53] I. Eisenberg, F. Caycedo-Soler, D. Harris, S. Yochelis, S. F. Huelga, M. B. Plenio, N. Adir, N. Keren, and Y. Paltiel, J. Phys. Chem. B **121**, 1240 (2017).

[54] D. Tamascelli, A. Segati, and S. Olivares, Int. J. Quantum Inf. **15**, 1740006 (2017).

[55] A. Davydov, *Theory of Molecular Excitons* (Plenum, New York, 1971).

[56] C. A. Schroeder, F. Caycedo-Soler, S. F. Huelga, and M. B. Plenio, J. Phys. Chem. A **119**, 9043 (2015).

[57] M. H. C. Koolhaas, R. N. Frese, G. J. S. Fowler, T. S. Bibby, S. Georgakopoulou, G. van der Zwan, C. N. Hunter, and R. van Grondelle, Biochemistry **37**, 4693 (1998).

[58] H. van Amerongen, L. Valkunas, and R. van Grondelle, *Photosynthetic Excitons* (World Scientific, Singapore, 2000).

[59] Y. Oshikane, T. Kataoka, M. Okuda, S. Hara, H. Inoue, and M. Nakano, Sci. Technol. Adv. Mater. **8**, 181 (2007).

[60] J. S. Paiva, P. A. Jorge, C. C. Rosa, and J. P. Cunha, Biochim. Biophys. Acta Gen. Subj. **1862**, 1209 (2018).

[61] P. W. Anderson, Phys. Rev. **109**, 1492 (1958).

[62] S. Jang, M. D. Newton, and R. J. Silbey, Phys. Rev. Lett. **92**, 218301 (2004).

[63] M. Escalante, A. Lenferink, Y. Zhao, N. Tas, J. Huskens, C. N. Hunter, V. Subramaniam, and C. Otto, Nano Lett. **10**, 1450 (2010).

[64] A. Mattioni, F. Caycedo-Soler, S. F. Huelga, and M. B. Plenio, arXiv:1812.07905.